



# Q1 Decomposition of brain diffusion imaging data uncovers latent 2 schizophrenias with distinct patterns of white matter anisotropy

Q2 Javier Arnedo<sup>a</sup>, Daniel Mamah<sup>b</sup>, David A. Baranger<sup>b</sup>, Michael P. Harms<sup>b</sup>, Deanna M. Barch<sup>b,c</sup>,  
4 Dragan M. Svrakic<sup>b</sup>, Gabriel Alejandro de Erausquin<sup>d</sup>, C. Robert Cloninger<sup>b,e</sup>, Igor Zvir<sup>a,b,\*</sup>

5 <sup>a</sup> Department of Computer Science and Artificial Intelligence, University of Granada, Spain

6 <sup>b</sup> Department of Psychiatry, Washington University School of Medicine, St. Louis, MO, USA

7 <sup>c</sup> Department of Psychology and Department of Anatomy & Neurobiology Washington University, St. Louis, MO, USA

8 <sup>d</sup> Roskamp Laboratory of Brain Development, Modulation and Repair, Department of Psychiatry and Behavioral Neurosciences (GAE), University of South Florida, Tampa, FL, USA

9 <sup>e</sup> Department of Genetics (CRC), Washington University School of Medicine, St. Louis, MO, USA

## 10 ARTICLE INFO

### 11 Article history:

12 Received 9 December 2014

13 Accepted 28 June 2015

14 Available online xxxx

### 15 Keywords:

16 Schizophrenias

17 White matter

18 Fractional anisotropy

19 Positive and negative symptoms

20 Biclusters

21 Generalized factorization

22 Non-negative Matrix Factorization

23 Model-based clustering

24 Consensus clustering

25 Fuzzy clustering

26 Possibilistic clustering

27 Relational clustering

28 Conceptual clustering

## ABSTRACT

Fractional anisotropy (FA) analysis of diffusion tensor-images (DTI) has yielded inconsistent abnormalities in 29 schizophrenia (SZ). Inconsistencies may arise from averaging heterogeneous groups of patients. Here we investigate 30 whether SZ is a heterogeneous group of disorders distinguished by distinct patterns of FA reductions. We 31 developed a Generalized Factorization Method (GFM) to identify biclusters (i.e., subsets of subjects associated 32 with a subset of particular characteristics, such as low FA in specific regions). GFM appropriately assembles a 33 collection of unsupervised techniques with Non-negative Matrix Factorization to generate biclusters, rather 34 than averaging across all subjects and all their characteristics. DTI tract-based spatial statistics images, which out- 35 put is the locally maximal FA projected onto the group white matter skeleton, were analyzed in 47 SZ and 36 36 healthy subjects, identifying 8 biclusters. The mean FA of the voxels of each bicluster was significantly different 37 from those of other SZ subjects or 36 healthy controls. The eight biclusters were organized into four more general 38 patterns of low FA in specific regions: 1) genu of corpus callosum (GCC), 2) fornix (FX) + external capsule (EC), 39 3) splenium of CC (SCC) + retrolenticular limb (RLIC) + posterior limb (PLIC) of the internal capsule, and 4) an- 40 terior limb of the internal capsule. These patterns were significantly associated with particular clinical features: 41 Pattern 1 (GCC) with bizarre behavior, pattern 2 (FX + EC) with prominent delusions, and pattern 3 42 (SCC + RLIC + PLIC) with negative symptoms including disorganized speech. The uncovered patterns suggest 43 that SZ is a heterogeneous group of disorders that can be distinguished by different patterns of FA reductions 44 associated with distinct clinical features. 45

© 2015 Published by Elsevier Inc. 46

## 49 Introduction

51 White matter lesions in the brain are generally associated with ab- 52 normal connectivity of brain regions in complex diseases such as schizo- 53 phrenia (SZ) (Lee et al., 2013; Liu et al., 2013; Skudlarski et al., 2013). It 54 has been reported that white matter abnormalities may suggest clues 55 relevant to the neurodevelopmental origin of these diseases (Huang 56 et al., 2011; Keller et al., 2007; Lee et al., 2013). To allow the investiga- 57 tion of white matter structural abnormalities in vivo, diffusion tensor 58 imaging (DTI) has been widely used; this magnetic resonance imaging 59 technique measures localized water diffusivity reflecting the geometric 60 properties and directionality of both the axonal membrane and myelin 61 in large white matter tracts of the brain (Mori, 2007). Fractional 62

anisotropy (FA) is a scalar measure often used in DTI, which describes 63 the directional dependence of diffusion (i.e., anisotropy); it is related 64 to axonal fiber density, axonal diameter and myelination in white 65 matter (Mori, 2007; Song et al., 2002). Unfortunately, DTI findings 66 in SZ have been inconsistent across studies (Alba-Ferrara and de 67 Erausquin, 2013; Kubicki et al., 2007). Specifically, studies have either 68 reported no white matter FA differences between controls and patients 69 with SZ (Foong et al., 2002; Suddath et al., 1990; Wible et al., 1995), 70 minimal regional FA abnormalities (Lee et al., 2013; Liu et al., 2013; 71 Skudlarski et al., 2013), or widespread FA abnormalities (Douaud 72 et al., 2007; Lim et al., 1999; Minami et al., 2003). 73

The inconsistencies in SZ studies may arise from averaging heteroge- 74 neous groups of patients with varying FA abnormalities (Fig. 1). Identi- 75 fication of relevant changes in FA is particularly challenging when 76 subjects vary extensively in their clinical features and severity, which 77 are likely to have complex relations with different brain structures 78 and functions (Blanchard and Cohen, 2006; Holliday et al., 2009). 79 Regional differences can be missed due to the fuzziness of the data, 80

\* Corresponding author at: Washington University School of Medicine, Barnes-Jewish Hospital (south), Renard Building 4940 Children's Place, Room 2202, Campus Box 8134, St. Louis, MO 63110, USA.

E-mail address: [zwir@psychiatry.wustl.edu](mailto:zwir@psychiatry.wustl.edu) (I. Zvir).

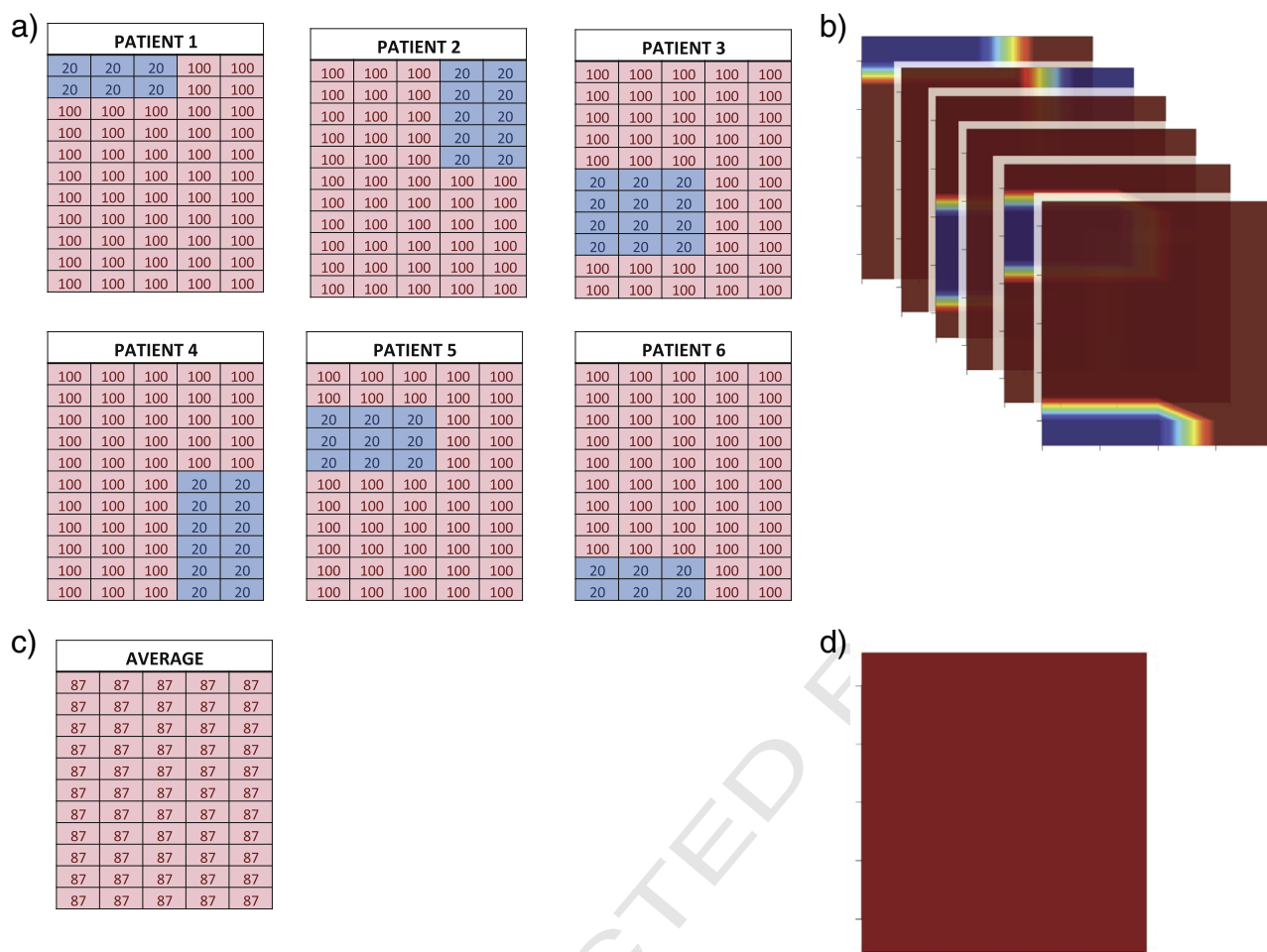


**Fig. 1.** Synthetic example of global and local tensor identification in patients. (a) Synthetic 2nd order tensor representation of TBSS images (i.e., x and y dimensions from subjects with different local abnormalities). (b) Voxelgrams corresponding to a 3rd order tensor representation of TBSS images in (a) (i.e., x, y, and subject dimensions). (c) Averaged values of all tensors in (a). (d) Voxelgram corresponding to (c).

particularly when the abnormality is mild (Alba-Ferrara and de Erausquin, 2013).

To characterize the heterogeneity of structural brain abnormalities in SZ, we devised an unsupervised machine learning approach that decomposes a collection of FA images from patients with SZ into local partitions or biclusters (Cichocki, 2009; Pascual-Montano et al., 2006b; Tamayo et al., 2007). These biclusters are composed of co-differentiated white matter FA sets of voxels (i.e., voxels with low FA values) shared by subsets of subjects. Biclustering captures local and intrinsic relationships between subsets of observations (subjects) sharing subsets of descriptive features (voxels) instead of relationships between all subjects and all their descriptive features. These relationships can be weakened when all features are used in a single global model of data, as is typically done by clustering methods.

Our approach combines the advantages of a number of complementary clustering strategies into a Generalized Factorization Method (GFM, Supplementary Fig. 1) and has been previously widely applied in different biomedical problems (Harari et al., 2010; Romero-Zaliz et al., 2008b; Zwir et al., 2005b). Non-negative Matrix Factorization (NMF) algorithms have also been utilized in facial recognition (Lee and Seung, 1999), gene expression (Tamayo et al., 2007), and several other biomedical problems (Cichocki, 2009). More recently, we successfully applied a composite GFM–NMF to uncover eight different subtypes of SZ by dissecting genome wide association studies into biclusters composed of distinct sets of genetic variants and clinical symptoms of SZ patients (Arnedo et al., 2013, 2014).

In the current study, we applied the GFM–NMF methodology to examine a sample of SZ patients and healthy controls whose diffusion-weighted brain images were processed using Tract Based Spatial Statistics (TBSS) (Smith et al., 2006). We refer to the output of TBSS, which is the locally maximal FA projected onto the group white matter skeleton, as an FA–TBSS image. We searched for biclusters reflecting different FA patterns that can be shared by distinct subsets of SZ patients. Then we evaluated the significance of each bicluster by comparing the differential FA within a bicluster with that exhibited by healthy controls, as well as with that shown in other individuals with SZ who were not present in the bicluster. We then analyzed the anatomical location of DTI abnormalities identified in the biclusters. In the final step, we cross-correlated the uncovered biclusters with collected descriptions of clinical features of the patients including positive and negative symptoms scores as defined by the Scale for the Assessment of Positive Symptoms (SAPS) and the Scale for the Assessment of Negative Symptoms (SANS) (Andreasen, 1984).

The method illustrated here is able to agnostically decompose FA–TBSS images and to distinguish subsets of SZ patients using white matter FA patterns, just as we decomposed SZ into subtypes with complex relations between sets of genotypes and sets of clinical phenotypes (Arnedo et al., 2014). These abnormalities may suggest distinct etiologies in patients diagnosed with SZ, characterized by different brain areas leading to distinct symptoms and clinical outcomes. The software is available upon request from the authors.

## Methods

### Study sample

The participants included in the study were drawn from a population of volunteers for studies of brain structure and function at the Conte Center for the Neuroscience of Mental Disorders at Washington University Medical School, St. Louis. All participants gave written informed consent for participation following a complete description of the risks and benefits of the study.

Participants consisted of 47 individuals (mean age = 37.2 yrs; SD = 8.5) who met DSM-IV (American Psychiatric Association, 1994) criteria for SZ, and outpatients at the time of study. Diagnosis was ascertained by consensus between a research psychiatrist, who conducted a semi-structured interview, and a trained research assistant who used the Structured Clinical Interview for DSM-IV Axis I Disorders (First et al., 2002). Participants were excluded if they: (1) met DSM-IV criteria for substance abuse or dependence within the past 6 months; (2) had a clinically unstable or severe medical condition, or a medical condition that would confound the assessment of psychiatric diagnosis (e.g., hypothyroidism); (3) had a history of head injury with neurological sequelae or loss of consciousness; or (4) met DSM-IV criteria for mental retardation (mild or greater in severity). Participants include 16 females and 31 males. Ethnically, they included 1 Asian, 26 Blacks/African Americans, 19 Caucasians, and 1 multiracial. Five participants were left handed, and the rest were right handed.

Control participants consisted of 36 individuals (mean age = 36.9 yrs; SD = 9.1) who did not meet criteria for DSM-IV schizophrenia, bipolar disorder, or major depression. Other exclusion criteria were the same as for the SZ subjects. Control participants included 19 females and 17 males. Ethnically, they included 24 Blacks/African Americans and 12 Caucasians. Two control participants were left handed, and 34 were right handed.

### Clinical measures

The presence and severity of positive (psychotic) symptoms was assessed using the Scale for the Assessment of Positive Symptoms (SAPS) (Andreasen, 1984). Negative symptoms were assessed using the Scale for the Assessment of Negative Symptoms (SANS) (Andreasen, 1984).

### Image acquisition and pre-processing

Magnetic resonance (MR) scans were obtained using a 3 T Siemens Tim Trio scanner with a 12-channel head coil. Structural images were acquired using a sagittal magnetization-prepared radiofrequency rapid gradient-echo 3D T1-weighted sequence (TR = 2400 ms, TE = 3.16 ms, flip angle = 8°, voxel size = 1 mm isotropic). Two DTI scans (each ~ 5 min) were acquired in an oblique–axial plane with a single shot echo-planar imaging (EPI) sequence with TR = 8000 ms, TE = 86 ms, FOV 224 × 224 mm<sup>2</sup>, 2 mm isotropic voxels (112 matrix with 64 slices of 2 mm), phase encoding in the A–P direction, 6/8 partial Fourier, and a parallel acceleration factor in the phase direction of 2 (GRAPPA = 2). Each DTI scan consisted of 30 volumes acquired with non-collinear diffusion-sensitizing directions at a b-value of 800 s/mm<sup>2</sup> and five interspersed volumes acquired without diffusion weighting (b-value = 0 s/mm<sup>2</sup>).

Data from the two DTI scans was concatenated and then pre-processed using FMRIB Software Library (FSL) version 4.1 (Nacsa et al., 2004). Briefly, within a given subject, a reference b = 0 volume was brain-extracted (Smith, 2002) and the diffusion-weighted volumes were registered to this reference to correct for movement and eddy current distortion (using FSL's 'eddy\_correct'). A diffusion tensor was derived at each voxel using a standard least-squares process (FSL's 'dtfit') to provide voxel-wise calculations of fractional anisotropy

(FA). As a quality control mechanism, the residual error between the calculated tensor model fit and original data was computed for each slice and volume. Volumes containing slices with poor model fits were removed from the data, and the tensor was recomputed without the problematic volumes. This is an effective mechanism to identify and remove volumes with artifacts due to motion or other scanner anomalies (e.g., signal loss due to the table vibration artifact discussed in Gallichan et al., 2010).

### DTI data analysis: Tract Based Spatial Statistics (TBSS)

TBSS was carried out using FSL 4.1 (Smith et al., 2006). All participants' FA data were projected onto a mean FA image using the non-linear registration tool FNIRT to register to the FMRIB58\_FA standard brain template. The registered data was thinned to create a mean FA skeleton restricted to voxels with the highest FA at the center of the major WM tracts. Following visual assessment of the optimal threshold value, the skeleton was thresholded at the recommended level of FA = 0.2 in order to remove confounding low-FA voxels, which may be caused by partial volume effects of gray matter or cerebrospinal fluid. Each participant's aligned FA data were projected onto the skeleton by searching the maximum FA value in a region perpendicular to the skeleton (FA-TBSS image). This projection was performed for every subject.

### Rationale of the Generalized Factorization Method (GFM) and the Non-negative Matrix Factorization method (NMF)

Our GFM was designed and successfully applied to identify structural patterns or clusters (substructures) that characterize complex objects embedded in databases (Cordon et al., 2002; Romero-Zalaz et al., 2008a; Ruspini and Zwir, 2002; Zwir et al., 2005a). Unfortunately, solving these kinds of complex problems cannot be resolved by a single clustering method but only by utilizing and combining the advantages of many of them, as we implemented in GFM and summarized below (Supplementary Fig. 1, see Supplementary Methods). NMF algorithms find an approximate factoring of the data:  $M \sim W_K \times H_K$ , where both decomposition matrices have only positive entries (Arnedo et al., 2013; Lee and Seung, 1999; Pascual-Montano et al., 2006b; Tamayo et al., 2007) (see Supplementary methods).  $W_K$  is an  $n \times K$  matrix that defines the sub-matrix decomposition model whose columns specify how much each of the subjects contributes to each of the  $K$  sub-matrices.  $H_K$  is a  $k \times m$  matrix whose entries represent the FA values in the  $k$  sub-matrices for each of the  $m$  voxels. Biclusters composed of distinct subsets of features/attributes shared by subsets of observations are derived from each sub-matrix. We integrated the GFM and NMF (GMF–NMF) to identify biclusters that can handle sparse, fuzzy and different data granularity (Cichocki, 2009).

### The GFM–NMF method: identifying biclusters in FA-TBSS images

This method distinguishes four main processes (Fig. 2) where FA-TBSS images from different subjects were appropriately encoded, and multiple biclusters were determined and evaluated based on quality measures (sensitivity, generality) to select an optimal descriptive set. During selection, niches are defined to run selection locally and provide diverse but still optimal biclusters. Finally, biclusters were topologically organized and decoded into NIFTI 3D images.

### Codification of the image database

Flattening each subject's FA-TBSS image produced a vector (e.g. [voxels × subject], Fig. 2) (Cichocki, 2009). These vectors were included as rows in matrix  $M$  using *oro.nifti* package, R version 2.15.1, where each row corresponded to a subject and each column to a tagged voxel (e.g., voxel\_ID). Here, 126,586 voxels were present in the TBSS skeleton, and those cells corresponding to voxels outside the TBSS skeleton were

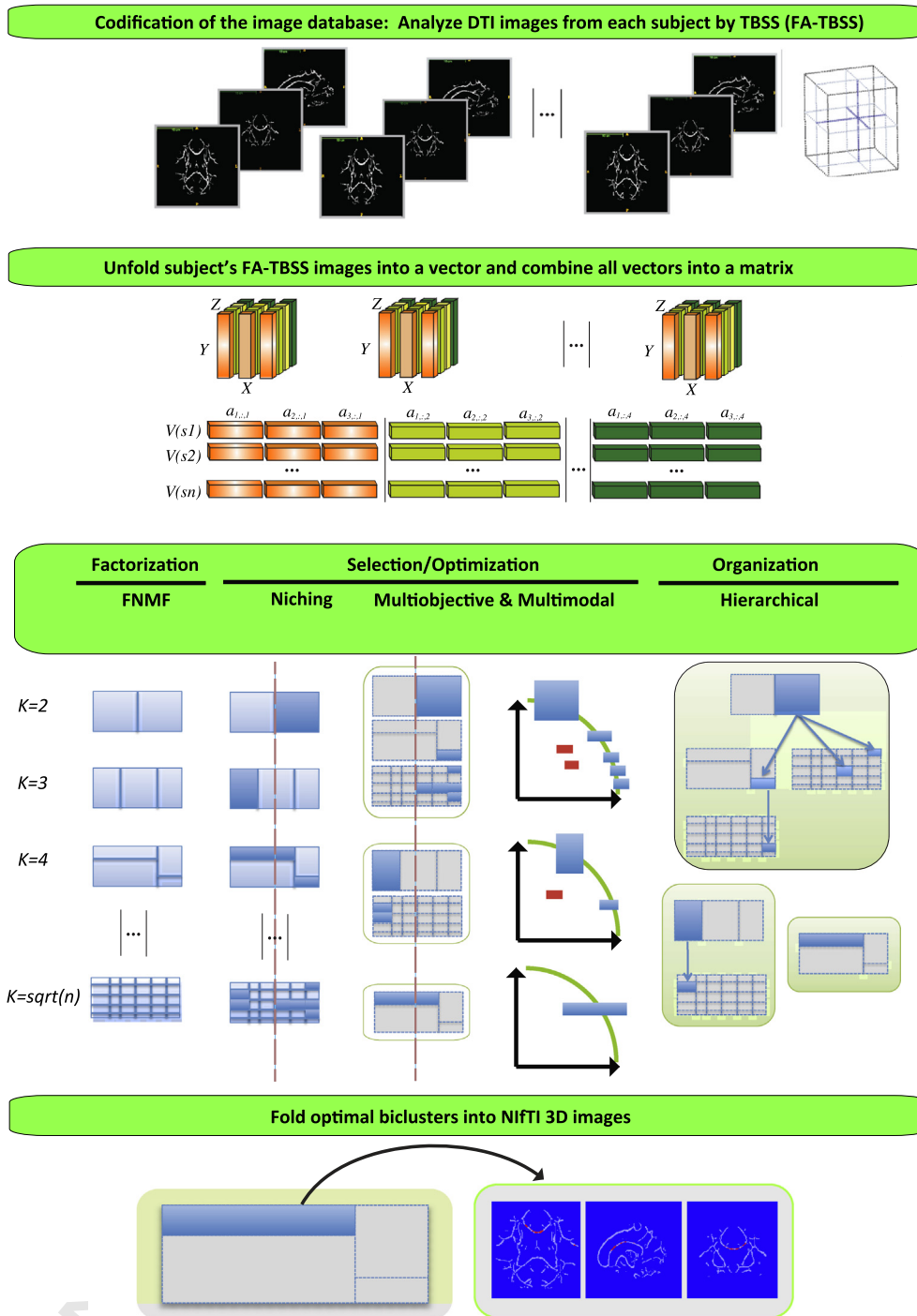


**Fig. 2.** The GFM-NMF method: identifying biclusters in FA-TBSS images. The method consists of four main steps: (1) codification of the image database; (2) factorization of the image database; (3) optimization and organization of the factorized image database; and (4) folding the optimal biclusters into NIFTI 3D images for visualization.

removed from the matrix. The tagging order was used for posterior reconstruction of the images (see step 4). (Note that the coordinates (x, y, z) of the voxels in the  $R^{X \times Y \times Z}$  space are not necessary for the comparison of their FA values and for reconstructing images from matrices in this particular problem.) For convenience, we utilized transposed ( $M^T$ ) and normalize matrix  $M$  by scaling each column in the [0, 1] interval Eq. (1):

$$a'_{x,y,z} = 1 - \frac{a_{x,y,z} - \text{Min}(a_{x,:z})}{\text{Max}(a_{x,:z}) - \text{Min}(a_{x,:z})}; \forall a_{x,y,z} \in M. \quad (1)$$

Here the assumption is that we were interested in identifying voxels with low values relative to the rest of the patients rather than in finding voxels with the global lowest FA values. Therefore, we reversed the ordering so that low FA values produced entries near 1. This approach facilitates the search of biclusters by NMF methods, which tend to favor groupings of high values.

*Factorization of the image database*

*Decomposition of the matrix  $M$  into sub-matrices  $M_k = 1, \dots, K$  using the FNMF implementation of the NMF method with default parameters as*



described in Arnedo et al. (2013), where  $K$  corresponds to the maximum numbers of possible sub-matrices (i.e., clusters). For  $K = 2$  to  $\sqrt{n}$ , where  $n$  is the number of subjects in the sample, apply FNM to  $M$  recurrently and calculate the corresponding  $H_K$  and  $W_K$  matrices. 40 different initializations of the FNM parameters were run before selecting the best results for a given  $K$  (see Sampling in Supplementary methods), which are normally enough runs to achieve internally robust sub-matrices (Arnedo et al., 2013; Pascual-Montano et al., 2006a,b).

**Identification of biclusters from FNM factorizations.** Select the most representative rows and columns in the  $H_K$  and  $W_K$  matrices, respectively, for each one of the  $k$ -factors (sub-matrices) independently. Sorting the rows in  $W_K$  for each column in descending order and selecting those rows that are higher than a given threshold achieves this (see below). Analogously, repeat the process for the  $H_K$  matrix to select the columns. The set of selected rows (subjects) and columns (voxels) for each factor define a bicluster  $B_k$ , with  $k = [1, \dots, K]$ .

The threshold (Eq. (2)) for factor  $k$  in the matrix  $H_K$  is defined in the unit interval  $[0-1]$  and calculated as:

$$\text{Threshold} = \max(H_K) * (1 - \delta) \quad (2)$$

with  $\delta$  being the degree of fuzziness of the bicluster. Here, a default  $\delta = 0.35$  was utilized, which is consistent with the typical 70–30%  $\pm$  5% partition of the holdout (2-fold crossvalidation) sampling method (Mitchell, 1997) (see sensitivity analysis of this parameter in Supplementary methods).

**Elimination of redundant biclusters.** Because FNM identifies biclusters in partitions with different number of clusters  $K$ , it is possible that the same bicluster can be generated more than one time. Biclusters with a high degree of overlap are considered once. The degree of overlap between two biclusters was assessed by calculating the pairwise probability of intersection among them based on the hypergeometric distribution ( $PI_{hyp}$ , Eq. (3)) (Tavazoie et al., 1999; Zwir et al., 2005a):

$$PI_{hyp}(B_i, B_j) = 1 - \sum_{q=0}^{p-1} \binom{h}{q} \binom{g-h}{n-q} / \binom{g}{h}; \quad h = |B_i|; n = |B_j|; p = |B_i \cap B_j| \quad (3)$$

where  $p$  observations (subjects)/features (voxels) belong to bicluster  $B_i$  with size  $h$ , and also belong to a bicluster  $B_j$  of size  $n$ ; and  $g$  is the total number of observations. Therefore, the lower the  $PI_{hyp}$ , the higher the overlapping and the better co-cluster coincidence. Here, a default  $PI_{hyp} < 1E-03$  was utilized (Arnedo et al., 2013; Tavazoie et al., 1999; Zwir et al., 2005b). Biclusters harboring <10% of the total number of subjects were not considered to avoid a trend to obtain singleton biclusters.

#### Optimization and organization of the factorized image database

**Evaluation of biclusters.** Biclusters were characterized by two objectives: specificity and generality. Specificity is defined as the frequency of voxels displaying low FA values in a bicluster relative to the entire FA-TBSS image (Eq. (4)):

$$\text{Specificity}(B_i) = \frac{\# \text{ voxels } \in B_i}{\# \text{ total voxels}} \quad (4)$$

where voxels in  $B_i$  correspond a subset of low FA values (Eq. (1)) shared by a particular subset of subjects, and *total voxels* correspond to the entire voxels in an FA-TBSS image (Eq. (4)). Here the assumption is that our data are sparse, and thus, large number of voxels may produce associations with diverse brain regions (suggesting low specificity), whereas a small number of voxels tend to be concentrated in a single or a few cohesive locations (suggesting high specificity) (Arnedo et al.,

2014; Cordon et al., 2002; Ruspini and Zwir, 2002; Zwir et al., 2005a). Generality is defined in the same fashion but with respect to the subjects in a bicluster (Eq. (5)):

$$\text{Generality}(B_i) = \frac{\# \text{ subjects } \in B_i}{\# \text{ total subjects}} \quad (5)$$

where subjects in  $B_i$  share particular subsets of voxels with low FA values. Here the assumption is that biclusters generated with a small maximum number of clusters  $K$  (low granularity) tend to include a large number of subjects, and thus, they are likely to share a more heterogeneous set of features (voxels with low FA values) than a smaller group of subjects from a bicluster generated when using a large  $K$  value (high granularity) (Arnedo et al., 2014; Cordon et al., 2002; Ruspini and Zwir, 2002; Zwir et al., 2005a, see sensitivity analysis of parameters in Supplementary methods).

Another indirect objective considered for the evaluation of biclusters is the generation of diverse patterns that completely describe objects (patients). Therefore, our approach evaluates the sensitivity and generality objectives described above in a local niche (Deb, 2001a,b; Ruspini and Zwir, 2002; Zwir et al., 2005a). Both sensitivity and specificity measurements are based on counting objects within a bicluster without distinguishing among them (e.g., # subjects). However, diversity differentiates which objects are within a bicluster, and thus, biclusters harboring distinct objects are allocated in different niches. These niches are calculated using Jaccard's metric between biclusters (Romero-Zaliz et al., 2008a,b) (i.e., inclusion of subjects, Eq. (6)):

$$\text{Niching}(B_i, B_j) = \frac{S(B_i) \cap S(B_j)}{S(B_i) \cup S(B_j)} > \gamma \quad (6)$$

where  $B_i$  and  $B_j$  were the two different biclusters, the  $S$  functional retrieves the subjects in the biclusters in a particular niche, and  $\gamma$  (0.7) is size of the niche determined by the degree of overlapping/intersection between biclusters. Here the assumption is that the niches are equivalence classes dictated by the degree of overlapping/inclusion between subjects in the biclusters.

**Selection of optimal biclusters using multiobjective and multimodal optimization techniques.** Optimal biclusters were obtained as a tradeoff between two opposing objectives: sensitivity and generality (Arnedo et al., 2014; Deb, 2001a,b; Ruspini and Zwir, 2002; Zwir et al., 2005a). A Pareto-optimization strategy searches for solutions that are non-dominated in the sense that there was no other solution superior in all objectives being selected (i.e., close to Minimum Description-Length (MDL) (Rissanen, 1989)). The dominance relationship as a minimization problem is defined as (Eq. (7)):

$$a < b \text{ iff } \forall i \ O_i(a) \leq O_i(b) \ \exists j \ O_j(a) < O_j(b) \quad (7)$$

where the  $O_i$  and  $O_j$  are either specificity or generality objectives. Optimization of small sets of biclusters was exhaustively implemented, whereas evaluation of large sets is approached by genetic algorithms, as described in Harari et al. (2010) and Romero-Zaliz et al. (2008a,b). MDL-like optimization approaches recommend the “best” model by optimizing the sum of the model accuracy and its size (single objective), and encode the information into bits. Pareto-based optimization solves the original multi-objective problem by treating the model-quality criteria of accuracy and size as two separate quality measures, and is more generic than MDL since it can cope with any kind of non-commensurable model-quality criteria (Freitas, 2004; Ruspini and Zwir, 2002; Zwir et al., 2005a).

Our approach applied the non-dominance relationship described above locally. That is, it identifies all non-dominated optimal biclusters that have no better solution (i.e., multiobjective) in a niche (i.e., multimodality) or equivalence class defined based on

the non-dominance partial order (Deb, 2001a; Ruspini and Zwir, 2002; Zwir et al., 2005a). Then, given two biclusters where one of them has the same or even worst sensitivity and generality than the other but correspond to different sets of subjects, both biclusters will be preserved because they are in different niches. Biclusters containing <10% of the total number of subjects were not considered to avoid a trend yielding singleton biclusters. Statistical significance was used as an independent validation measurement of the bicluster quality (see below).

*Topological organization of optimal biclusters into hierarchies.* Non-dominated biclusters in each niche were top-down organized into hierarchies (networks or sub-graphs) from the most general (i.e., the bicluster containing the greatest number of subjects, see above) to the most specific (i.e., the bicluster containing the smallest and most cohesive set of voxels, as described above). Note that one bicluster can belong to more than one niche based on the *Niching* function described above, or hierarchies can be disjoint when mapping to independent sets of subjects. Biclusters are renamed as  $B_{i,j}$ , where  $i$  corresponds to a particular hierarchy, and  $j$  to the order in such hierarchy (smallest  $j$ -value indicates the most general and top level bicluster).

*Folding the optimal biclusters into Nifti 3D images for visualization*

A new Nifti 3D image was generated for each bicluster from its corresponding matrix representation to visualize the location of specific FA voxels on the FA-TBSS images using the *oro.nifti* package in R version 2.15.1. The tagging order (voxel\_ID, see step (1)) used for encoding FA-TBSS images was utilized in a reverse fashion.

*Sensitivity analysis of parameters*

Comparisons between algorithms (i.e., the bioNMF and the FNMFBiclustering methods) and evaluation of parameters, including initialization and stopping criteria, outlier detection, number of clusters, and degree of fuzziness in the NMF methods are described in Supplementary Methods.

*Sampling analysis*

Sampling analysis was performed by leave-one-out and leave-one-bicluster-out as described in Supplementary methods.

*Statistical analysis*

Statistical analysis was performed by using one-way ANOVA, pairwise t-test and Bonferroni correction (R version 2.15.1) as described in Supplementary methods.

**Statistical analysis**

Identification of biclusters was unbiased without a prior knowledge of the anatomical location of voxels and/or the clinical symptoms of the subjects. Using internal criteria in cluster evaluation is biased towards algorithms that use the same cluster model (Bezdek, 1998). Therefore, external evaluations based on criteria that were not used for clustering, such as tests based on ANOVA and its F-statistic, are often added to the cluster evaluation (Färber et al., 2010). To assess the statistical significance of the findings, we compared the average FA in the set of voxels of each bicluster with the average FA value in the same voxels of either SZ subjects who were not included in the bicluster or healthy controls by one-way ANOVA and pairwise t-test (R version 2.15.1) and applying Bonferroni correction. Evaluation of global differences in FA between all patients and all controls has been performed in the same fashion. One factor ANOVA using GLM-univariate was used to test the interactions of FA reduction and gender in each hierarchy by creating a new two-level variable named “interact” (voxels  $\times$  proportion of gender in a bicluster). (Hierarchies were utilized to account for a larger number of

observations.) The obtained results cannot reject the null hypothesis of a different proportion of a particular gender than that of the original sample in each hierarchy (p-value > 0.1, after correction for multiple test,  $B_{1,1}$  was omitted since it has only 5 members).

## Results

*Biclusters encode sets of voxels with FA reductions shared by subsets of subjects with SZ*

We first investigated decreased FA regions in a sample composed of TBSS images from 47 SZ patients, which together did not exhibit significant differences from a similar sample composed of 36 images of healthy controls (see *Statistical analysis, Methods*, p-value > 0.81). A partition of the images corresponding to the patients with SZ using GFM-NMF uncovered eight optimal local partitions or biclusters, where each bicluster encoded a subset of subjects characterized by a similar degree of FA reduction in a particular subset of voxels. This method allowed any given subject and/or voxel to belong to more than one bicluster or to none of them (see *Methods*). The mean FA of the voxels in each of the eight biclusters significantly differed from the mean FA for voxels in the same location in either the other SZ subjects not included in that bicluster or from the healthy controls after correction for multiple comparisons (see *Statistical analysis, Methods, Table 1, Figs. 3–4*). This suggests that the biclusters should separately explain a large part of the variability in the population. In fact, 41 of the 47 SZ subjects were included in at least one bicluster (Table 1), which accounted for >95% of the FA variance across subjects (in the population) and suggests a high degree of generality.

The biclusters varied in terms of their size, based on the associated numbers of subjects and shared voxels. For example, one general bicluster (i.e., one having high coverage) contained 21 subjects and 9744 voxels, while another specific bicluster (i.e., one having low coverage) contained only 5 subjects and 1322 voxels. While generality implies a large coverage of the sample; specificity displays smaller but more cohesively arranged and shared sets of FA voxels in the sample. The latter two biclusters did not overlap, and thus were associated with FA reductions in different brain regions, as expected. On the other hand, another pair of biclusters containing 15 subjects with 5147 voxels and 5 subjects with 2637 voxels respectively, showed a high degree of overlap, describing FA reductions in similar brain regions but with distinct degrees of specificity and generality (Fuzzy clustering (Bezdek, 1981)). These results suggests that the biclusters uncovered by GFM vary and are optimal in terms of their specificity and generality, as well as diversity, which is exemplified by the brain region described by them (see *Methods*).

*Topological organization of biclusters uncovers functionally meaningful local regions of FA reduction*

Because the identification of biclusters is not constrained by predefined knowledge about the anatomical region of the voxels, any grouping strategy may eventually identify sets of subjects sharing low FA values in voxels scattered throughout the whole brain. To evaluate the biological meaningfulness of FA reduction regions uncovered in the biclusters, our method topologically organized the eight biclusters into four main equivalence classes. The equivalence classes are defined by the partial order imposed by the non-dominance relationship among biclusters, that is, there is no better solution in both sensitivity and generality within each class (see *Methods*). Although “equivalent”, optimal biclusters within (and eventually across) these classes can be ordered on the basis of the inclusion of their subjects (Jech, 2003; Romero-Zaliz et al., 2008a; Zwir et al., 2005a,b) (see *Methods, Table 1, and Supplementary Fig. 2*). This organization of the classes is termed hierarchies, where biclusters located at the top and at the bottom of a hierarchy correspond to the most general and to the most specific

**Table 1**

Hierarchies containing biclusters uncovered by the GFM–NMF and their statistical significance (biclusters in bold are specifically illustrated in Fig. 5, and all biclusters are hierarchically shown in Supplementary Fig. 2).

Hierarchies <sup>*1</sup> /biclusters	#Subjects	#Voxels	Anatomical location	ANOVA F-test <sup>*2</sup>	Multiple comparison T-test <sup>*3</sup>	
					Controls	Rest of patients
<b>B<sub>1,1</sub></b>	5	1322	GCC	4.07E–04	5.40E–04	2.90E–04
<b>B<sub>2,1</sub></b>	15	5147	FX, EC	1.17E–07	7.20E–05	5.40E–08
<b>B<sub>2,2</sub></b>	7	3379	FX	2.63E–05	1.80E–04	1.40E–05
<b>B<sub>2,3</sub></b>	5	2637	FX	1.92E–03	4.90E–03	1.30E–03
<b>B<sub>3,1&amp;4,1</sub></b>	21	9744	ALIC, PLIC	5.89E–09	1.50E–04	2.50E–09
<b>B<sub>3,2</sub></b>	9	2569	SCC, PLIC, RLIC	1.13E–07	1.50E–05	5.20E–08
<b>B<sub>3,3</sub></b>	6	974	SCC, PLIC, RLIC	7.05E–04	2.89E–03	4.40E–04
<b>B<sub>4,2</sub></b>	11	1200	ALIC	1.01E–04	6.70E–04	6.80E–05

<sup>\*1</sup>B<sub>i,j</sub> indicates bicluster *j* in the hierarchy *i*.

<sup>\*2</sup>F-test corresponds to the p-value derived from the cdf of F-statistic in the one-way ANOVA (R version 2.15.1, aov()).

<sup>\*3</sup>T-test corresponds to the p-value derived from pairwise comparisons of means by T-test corrected by Bonferroni (R version 2.15.1, pairwise.t.test()).

biclusters, respectively. Moreover, all biclusters in a hierarchy are optimal in the sense that one bicluster is not worse (i.e., dominated) than another in both the objectives of specificity and generality (i.e., see multiobjective/multimodal optimization (Deb, 2001a,b; Zwir et al., 2005a,b), Methods, Table 1). Disjoint hierarchies indicate diversity of biclusters, and thus provide a distributed coverage and description of the sample.

Re-mapping of FA reduction regions from biclusters onto the original TBSS images, revealed that voxels with decreased FA tended not to be scattered but to be confined to certain areas for each hierarchy, and were localized to white matter tracts potentially relevant to the pathophysiology of SZ (Fig. 5). The four identified hierarchies

mapped to different anatomical regions (see Fig. 1 in Huang et al., 2011), Fig. 5).

The first hierarchy involved only one bicluster with decreased FA primarily in the genu of the corpus callosum (GCC) (Table 1, Fig. 5a). The second hierarchy included biclusters with patients involving FA reductions primarily in the fornix (FX) and/or in the external capsule (EC) (Table 1, Fig. 5b). The most general bicluster in this hierarchy included patients with FA reduction in both FX and EC, whereas another more specific bicluster in the same hierarchy differentiated a subset of patients with FA reduction only in the FX. The third hierarchy included biclusters with FA reductions in the retrolenticular limb of internal capsule (RLIC), and/or in the posterior limb of internal capsule (PLIC),

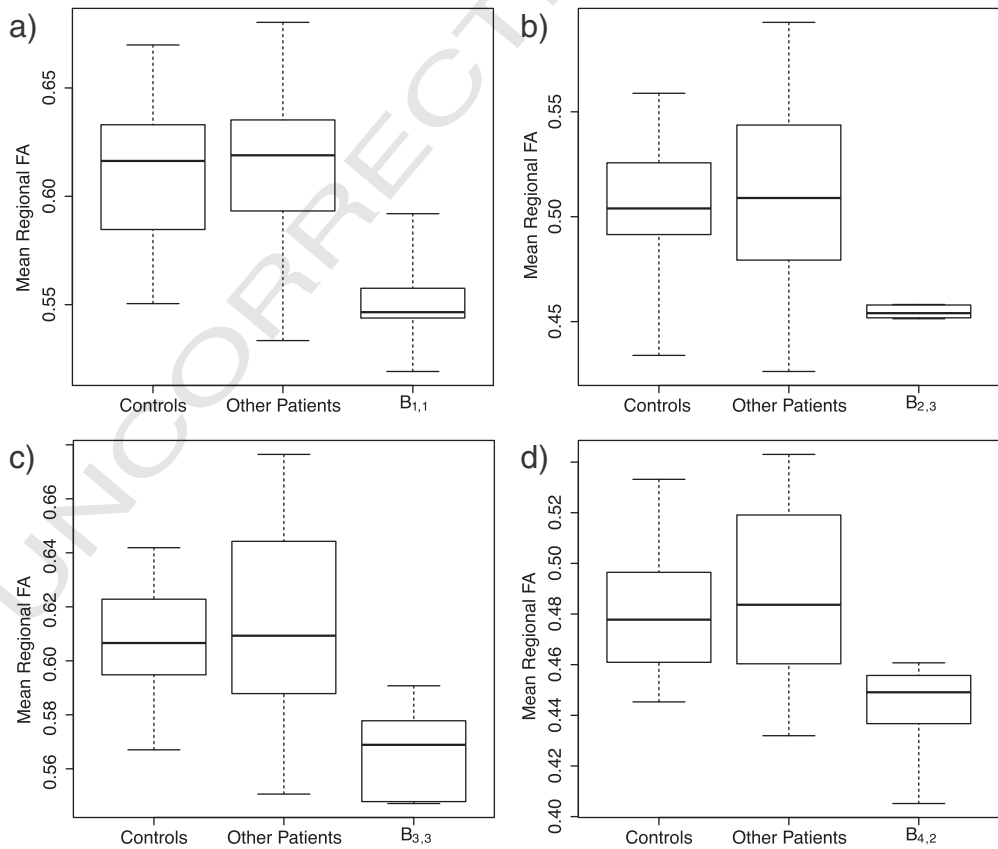


**Fig. 3.** Comparison of average FA values of four different biclusters. Box plots depict average FA values of four biclusters compared to identically located FA voxel values in SZ subjects who were not included in each specific bicluster and in healthy controls. Calculations were performed by one-way ANOVA (R version 2.15.1, function aov(), Table 1). Biclusters are renamed as B<sub>i,j</sub>, where *i* corresponds to a particular hierarchy, and *j* to the order in such hierarchy (smallest *j*-value indicates the most general and top level bicluster). (a) Comparisons for bicluster B<sub>1,1</sub>. (b) Comparisons for bicluster B<sub>2,3</sub>. (c) Comparisons for bicluster B<sub>3,3</sub>. (d) Comparisons for bicluster B<sub>4,2</sub>.

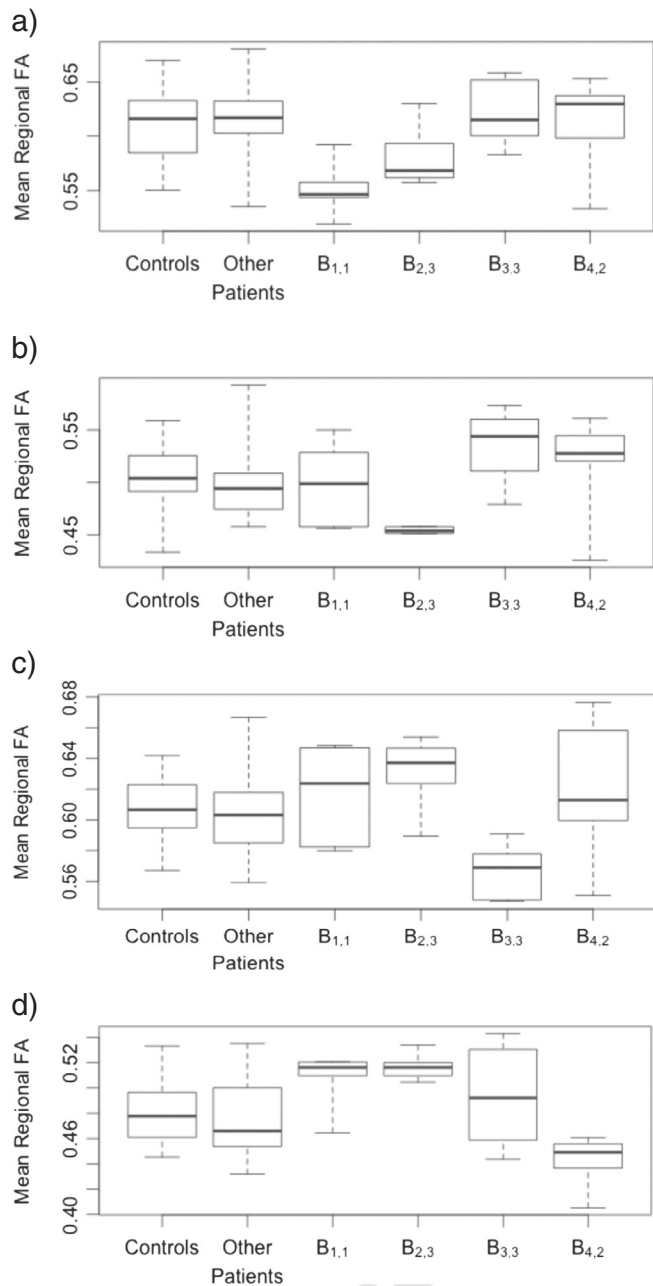


**Fig. 4.** Expanded comparison of average FA values of the four different biclusters described in Fig. 3. Box plots depict average FA values of four biclusters compared to identically located FA voxel values in all other SZ subjects, SZ subjects in the other biclusters, and healthy controls. Calculations were performed using one-way ANOVA (R version 2.15.1, *function aov()*). Biclusters are renamed as  $B_{i,j}$ , where  $i$  corresponds to a particular hierarchy, and  $j$  to the order in such hierarchy (smallest  $j$ -value indicates the most general and top level bicluster). (a) Comparisons for bicluster  $B_{1,1}$  (ANOVA  $p$ -value < 1.39E-03). (b) Comparisons for bicluster  $B_{2,3}$  (ANOVA  $p$ -value < 1.50E-03). (c) Comparisons for bicluster  $B_{3,3}$  (ANOVA  $p$ -value < 1.42E-04). (d) Comparisons for bicluster  $B_{4,2}$  (ANOVA  $p$ -value < 7.48E-06). Remarkably, the average FA values of biclusters  $B_{1,1}$  and  $B_{2,3}$  are higher – instead of lower – than the TBSS mean exhibited by the controls and the rest of the patients when voxels of the fourth (d) bicluster are evaluated.

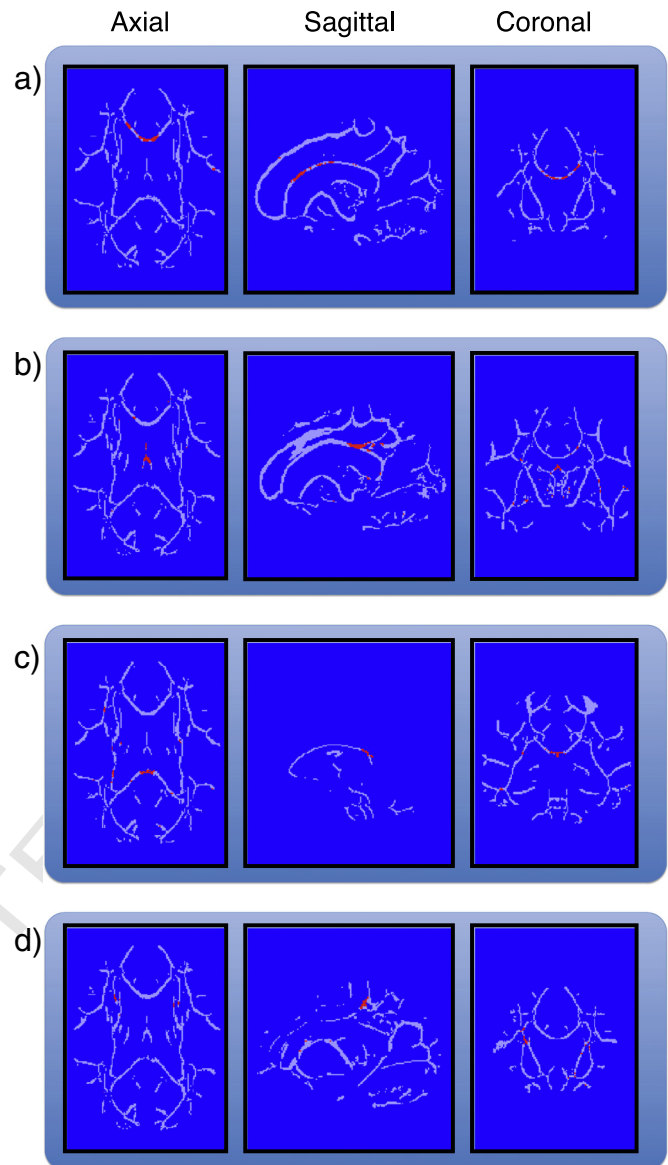


**Fig. 5.** Representation of low FA regions in white matter for different biclusters. Figures depict axial, sagittal, and coronal slice representations (left to right panels) of four biclusters mapping specific structural abnormalities (i.e., low FA), to regions on the brain white matter tracts. The utilized convention is that the right side corresponds to the right of the image. Gray pixels represent voxels included in the TBSS skeleton. Red pixels represent voxels from the TBSS skeleton that were identified by the corresponding biclusters (see Table 1). Biclusters are renamed as  $B_{i,j}$ , where  $i$  corresponds to a particular hierarchy, and  $j$  to the order in such hierarchy (smallest  $j$ -value indicates the most general and top level bicluster). (a) Representation of Bicluster  $B_{1,1}$ . (b) Representation of Bicluster  $B_{2,3}$ . (c) Representation of Bicluster  $B_{3,3}$ . (d) Representation of Bicluster  $B_{4,2}$ .

the other biclusters (Table 1, Figs. 3–4), showing FA reductions in the anterior limb of internal capsule (ALIC, Fig. 5d).

*Post hoc analysis of the subjects identified by disjoint biclusters uncovers distinct subsets of SZ patients with slightly different phenotypes*

To evaluate associations of each hierarchy's FA reductions with clinical features, we analyzed scores of SAPS and SANS items and domains (Supplementary Table 1, Fig. 6). Subjects within the first hierarchy were more likely to have certain bizarre behavior symptoms (i.e., social–sexual behavior, aggressive behavior), certain formal thought disorder symptoms (i.e., derailment and pressured or distractible speech), and delusions of reference (Supplementary Table 1, Fig. 6). These symptoms were significantly associated with the bicluster exhibiting FA reduction in the GCC



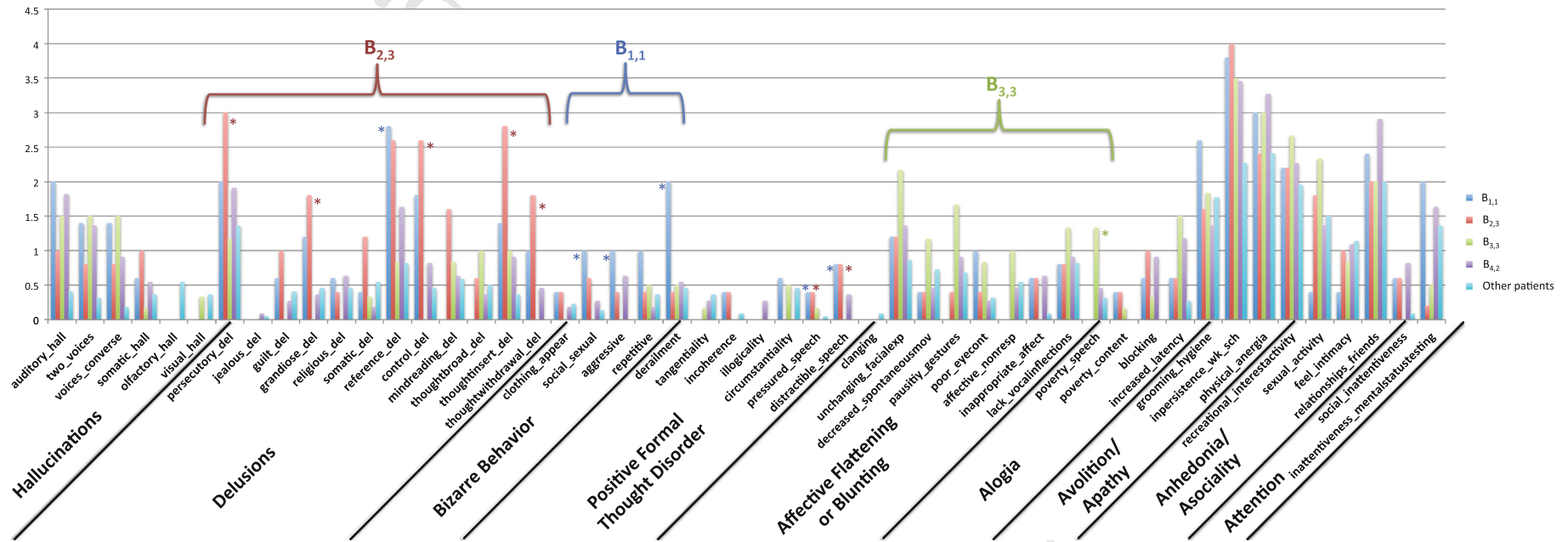


**Fig. 6.** Clinical relationships of biclusters. The bar plots show the averaged severity of positive (psychotic) symptoms (SAPS and SANS scales) for subjects included in bicluster  $B_{1,1}$  (blue bars), bicluster  $B_{2,3}$  (red bars), bicluster  $B_{3,3}$  (green bars), bicluster  $B_{4,2}$  (purple bars), and the rest of the patient sample (light blue bars). Biclusters are renamed as  $B_{ij}$ , where  $i$  corresponds to a particular hierarchy, and  $j$  to the order in such hierarchy (smallest  $j$ -value indicates the most general and top level bicluster). Significant differences in means of items exhibited by subjects of a particular bicluster are indicated with an asterisk (detailed statistics are indicated in Supplementary Table 1). Three sets of symptoms were linked with particular biclusters: delusion, bizarre behavior, and affective flattening or alogia symptoms were associated primarily with bicluster  $B_{2,3}$  (red brace), bicluster  $B_{1,1}$  (blue brace), and bicluster  $B_{3,3}$  (green brace), respectively. SAPS and SANS items are grouped by their corresponding domains.

the item level ( $p$ -value  $< 5.00E - 02$ , Supplementary Table 1) and at the domain level (e.g., bizarre behavior,  $p$ -value  $< 1.88E - 02$  after correction for multiple tests, Supplementary Table 2).

The second hierarchy was significantly associated (Supplementary Table 1, Fig. 6) with certain types of delusions (i.e., delusions of persecution, delusions of grandeur, delusions of control, mind reading delusions, thought insertion, and thought withdrawal). Although there was consistency across all clinical features in this hierarchy, specific biclusters showing FA reduction only in the FX were associated with more symptoms at the item level than general biclusters ( $p$ -value  $< 5.00E - 02$ , Supplementary Table 1) and at the domain level (e.g., delusions,  $p$ -value  $< 1.29E - 02$  after correction for multiple tests, Supplementary Table 2). This was expected because fewer individuals tend to have more features in common than larger sets of individuals. Subjects in biclusters associated with the third hierarchy were more likely to have poverty of speech and carelessness in their social and physical behavior ( $p$ -value  $< 5.00E - 02$ , Supplementary Table 1, Fig. 6). Finally, the fourth hierarchy did not have significant associations with any symptoms after Bonferroni corrections.

## Discussion

Studies of white matter using diffusion weighted MRI in SZ have reported decreased FA in many regions, but increased FA in some tracts has also been reported (Douaud et al., 2007; Kubicki et al., 2007). Findings about the degrees of FA in the literature have also been inconsistent. Recently, both a meta-review (Shepherd et al., 2012) and a large meta-analysis (Haijma et al., 2013) failed to find consistent reductions in white matter. White matter abnormalities in SZ may be progressive (Whitford et al., 2007), and a lack of uniformity in the stage of the disorder assessed may also account for some of the variability across studies. In the present work, we demonstrated that inconsistencies may also arise from using analytic methods that perform comparisons between averaged SZ and healthy control groups, which weakened possible differential FA reductions (Fig. 1) (Alba-Ferrara and de Erausquin, 2013).

Lower FA values have been reported by most SZ studies and in most white matter tracts (Cookey et al., 2014; Kubicki and Shenton, 2014). Even though increased FA has been reported in some tracts in SZ (Alba-Ferrara and de Erausquin, 2013), we decided to focus on low FA as a measure of the disconnectivity of particular tracts and to test if differences in FA were sufficient to uncover subsets of individual persons with distinct subtypes of the disease. FA was a particularly attractive measure because of it has high reliability (mean ICC = 0.70) and is more reproducible than alternative diffusion measures, including mean diffusivity, primary diffusivity and transverse diffusivity (Duan et al., 2015). Likewise, we selected TBSS as the approach to analyze these group differences for two reasons: first, it is widely used for this purpose, including comparisons between deficit and non-deficit syndromes (Spalletta et al., 2015), studies in first episode patients (Alvarado-Alanis et al., 2015), comparisons with bipolar disorder (Kumar et al., 2015), and assessment of the effects of medications (Ozcelik-Eroglu et al., 2014); second, TBSS methods are sensitive to longitudinal changes in brain white matter in neuropsychiatric disorders (e.g., Poudel et al., 2015).

We introduced an unsupervised machine learning approach (Mitchell, 1997) here termed GFM-NMF that decomposes a collection of images from different SZ patients into local partitions or biclusters (Madeira and Oliveira, 2004). This approach constructively combines the strength of different clustering algorithms (Supplementary Fig. 1) into a single method (Fig. 2) that exhibits flexibility and robustness in terms of critical parameters (e.g., number of clusters, degree of fuzziness) that often affect and, in turn, conceal the discovery of realistic patterns. Using our method, we identified several distinct patterns of FA reductions in SZ patients in a purely data-driven and unbiased manner. These patterns encoded as biclusters are optimal in terms of their specificity, sensitivity, and diversity. FA in brain regions of each bicluster was significantly different than

those of the same regions in the rest of the subject sample and in the controls. In addition, the derived biclusters remapped into 3rd order tensors represented as NIfTI 3D images, revealing that the biclusters were anatomically localized to white matter regions often associated with SZ (Lee et al., 2013; Liu et al., 2013; Skudlarski et al., 2013).

We identified low FA voxels in specific biclusters corresponding to discrete anatomical locations (i.e., GCC, SCC, FX, RLIC, PLIC, EC, and ALIC), which have been previously implicated in the pathophysiology of SZ. Biclusters in the first and second hierarchies are consistent with published studies reporting lower FA values in the GCC and the FX have been reported in first-episode SZ patients (Lee et al., 2013). Abnormalities within the GCC reported in SZ are thought to affect inter-hemispheric communications (Sivagnanasundaram et al., 2007), whereas the FX is the major outflow pathway of the hippocampus (Fitzsimmons et al., 2009). The subjects in biclusters associated with decreased FA in the GCC were characterized primarily by disorganized symptoms. In contrast, subjects associated with FA reduction in FX were noted to have prominent delusions. Lastly, biclusters in the third hierarchy were associated with abnormalities in the SCC, and a relatively higher severity of negative symptoms. Correlations between biclusters and clinical features may be a direct consequence of a role of the specific white matter abnormalities in producing symptoms. This may suggest distinct underlying etiologies in different patients diagnosed with SZ. In other words, distinct classes of schizophrenia can be characterized by abnormalities in different brain regions, just as we have shown elsewhere that different classes of schizophrenia can be distinguished by distinct sets of genes and distinct sets of clinical features (Arnedo et al., 2014). Our studies thus suggest that uncovering voxel-based biclusters in SZ show promise in reducing heterogeneity that is usually concealed in groups of people with the diagnosis of SZ.

Our method pursuing local partitions of brain images provides substantial advantages over classical clustering approaches. Averaging and comparing groups would be expected to miss real differences in FA if reductions are localized in different locations in each patient (Fig. 1). In contrast to classical clustering techniques, such as hierarchical clustering (Sokal and Michener, 1958) and k-means clustering (Hartigan and Wong, 1979), we used biclustering techniques that do not require patients in the same bicluster to perform similarly over all voxels exhibiting FA reduction. Classical clustering methods derive a global model whereas biclustering algorithms produce a local model in which signals emerge only in relevant dimensions.

Moreover, our approach does not require any assumption about the number of the patterns or biclusters. Establishing the optimal number of biclusters is an unsolved computational problem since different features emerge from different assumptions about this number (Bittner and Smith, 2003; Fraley and Raftery, 1998; Fred and Jain, 2005; Latorre Carmona et al., 2013). Our method uncovers optimal biclusters defined in distinct granular partitions (e.g., multi-way/hierarchical tensor decomposition (Cichocki, 2009)) defined based on a distinct number of clusters without being exhaustive or redundant. Optimality was defined as a trade-off among specificity, generality, and diversity of the biclusters by multiobjective optimization.

We recently characterized different types of SZ by describing its heterogeneous genotypic and phenotypic architecture (Arnedo et al., 2014). Here, we confirmed such heterogeneity by uncovering distinct brain abnormalities associated with different phenotypes. The limitation of our approach is clearly dictated by the quality of the data, particularly in the phenotypic measurements. This problem is exacerbated in psychiatric disorders due to the clinical condition of the patients at the evaluation, the different scales and questionnaires utilized, and the fuzziness intrinsic to the symptoms being evaluated. These constraints often impede detection of significant relationships between brain abnormalities and phenotypic symptoms. In contrast, our results show that the uncovered biclusters are associated with different sets of clinical features of SZ as well as having statistically significant FA reductions in particular anatomical regions with functions relevant to the

associated symptom patterns (Blanchard and Cohen, 2006; Holliday et al., 2009). Specifically the first group of subjects in the hierarchy displayed prominent bizarre behavior, the second group in the hierarchy displayed prominent delusions, and the third displayed prominent negative symptoms including disorganized speech (Supplementary Table 1, Fig. 6).

Together, our purely data-driven approach uncovered biclusters with statistically significant association between particular brain regions and distinct clinical features. The statistically significant and distinct clinical associations suggest that the biclusters are not a computational artifact. Therefore our results may provide clues about distinct pathophysiological processes that produce different forms of SZ. Our current method represents a novel approach to uncover latent patterns of whole-brain structural connectivity from DTI-derived TBSS data, and allows us to characterize complex relationships between different brain structures and functions with distinct sets of behavioral and cognitive features. This approach may be a pioneering contribution towards a foundation for precise person-centered diagnosis and treatment of psychotic disorders.

## Q9 Uncited reference

Arnedo et al., 2015

## Acknowledgments

This work was supported in part by the Spanish Ministry of Science and Technology TIN2009-13950, TIN2012-38805 including FEDER funds, the R.L. Kirschstein National Research Award to I.Z.; the National Institutes of Health including grant 5K08MH077220 to G.AdeE; K08MH085948 to D.M., and the National Institute of Mental Health MH066031 to D.M.B. G.A.deE is a Stephen and Constance Lieber Investigator, and Sidney R. Baier Jr. Investigator, as well as Roksamp Chair of Biological Psychiatry at USF.

## Financial disclosures

The authors report no financial relationships with commercial interest.

## Appendix A. Supplementary data

Supplementary data to this article can be found online at <http://dx.doi.org/10.1016/j.neuroimage.2015.06.083>.

## References

- Alba-Ferrara, L.M., de Erausquin, G.A., 2013. What does anisotropy measure? Insights from increased and decreased anisotropy in selective fiber tracts in schizophrenia. *Front. Integr. Neurosci.* 7, 9.
- Alvarado-Alanis, P., Leon-Ortiz, P., Reyes-Madrugal, F., Favila, R., Rodriguez-Mayoral, O., Nicolini, H., Azcarra, M., Graff-Guerrero, A., Rowland, L.M., de la Fuente-Sandoval, C., 2015. Abnormal white matter integrity in antipsychotic-naïve first-episode psychosis patients assessed by a DTI principal component analysis. *Schizophr. Res.* 162, 14–21.
- American Psychiatric Association, 1994. *Diagnostic and Statistical Manual of Mental Disorders*. American Psychiatric Publishing Inc., Washington, DC.
- Andreasen, N.C., 1984. *Scale for the Assessment of Positive Symptoms (SAPS)*. University of Iowa, Iowa City.
- Arnedo, J., del Val, C., de Erausquin, G.A., Romero-Zalaz, R., Svrakic, D., Cloninger, C.R., Zwir, I., 2013. PGMRA: a web server for (phenotype × genotype) many-to-many relation analysis in GWAS. *Nucleic Acids Res.* 41, 75.
- Arnedo, J., Romero-Zalaz, R., Zwir, I., Del Val, C., 2014. A multiobjective method for robust identification of bacterial small non-coding RNAs. *Bioinformatics* 30, 2875–2882.
- Arnedo, J., Svrakic, D.M., Del Val, C., Romero-Zalaz, R., Hernandez-Cuervo, H., Fanous, A.H., Pato, M.T., Pato, C.N., de Erausquin, G.A., Cloninger, C.R., Zwir, I., 2015. Uncovering the hidden risk architecture of the schizophrenias: confirmation in three independent genome-wide association studies. *Am. J. Psychiatry* 172 (2), 139–153.
- Bezdek, J.C., 1981. *Pattern Recognition With Fuzzy Objective Function Algorithms*. Plenum Press.

- Bezdek, J.C., 1998. Pattern analysis. In: Pedrycz, W., Bonissone, P.P., Ruspini, E.H. (Eds.), *Handbook of Fuzzy Computation*. Institute of Physics, Bristol, pp. F6.1.1–F6.6.20.
- Bittner, T., Smith, B., 2003. A theory of granular partitions. *Foundations of Geographic Information Science* 117–151.
- Blanchard, J.J., Cohen, A.S., 2006. The structure of negative symptoms within schizophrenia: implications for assessment. *Schizophr. Bull.* 32, 238–245.
- Cichocki, A., 2009. *Nonnegative Matrix and Tensor Factorizations: Applications to Exploratory Multi-way Data Analysis and Blind Source Separation*. John Wiley, Chichester, U.K.
- Cookey, J., Bernier, D., Tibbo, P.G., 2014. White matter changes in early phase schizophrenia and cannabis use: an update and systematic review of diffusion tensor imaging studies. *Schizophr. Res.* 156, 137–142.
- Cordon, O., Herrera, F., Zwir, I., 2002. Linguistic modeling by hierarchical systems of linguistic rules. *IEEE Trans. Fuzzy Syst.* 10, 2–20.
- Deb, K., 2001a. *Multi-objective Optimization Using Evolutionary Algorithms*. 1st ed. John Wiley & Sons, Chichester, New York.
- Deb, K., 2001b. Nonlinear goal programming using multi-objective genetic algorithms. *J. Oper. Res. Soc.* 52, 291–302.
- Douaud, G., Smith, S., Jenkinson, M., Behrens, T., Johansen-Berg, H., Vickers, J., James, S., Voets, N., Watkins, K., Matthews, P.M., James, A., 2007. Anatomically related grey and white matter abnormalities in adolescent-onset schizophrenia. *Brain* 130, 2375–2386.
- Duan, F., Zhao, T., He, Y., Shu, N., 2015. Test–retest reliability of diffusion measures in cerebral white matter: a multiband diffusion MRI study. *J. Magn. Reson. Imaging* 41, 1333–1336.
- Färber, I., Günemann, S., Krieger, H., Kröger, P., Müller, E., Schubert, E., Seidl, T., Zimek, A., 2010. On using class-labels in evaluation of clusterings. In: SIGKDD A. (Ed.), *MultiClust: Discovering, Summarizing, and Using Multiple Clusterings*. 751–752.
- First, M.B., S.R.L., Gibbon, M., Williams, J.B.W., 2002. *Structured Clinical Interview for DSM-IV Axis I Disorders, Research Version, Patient Edition (SCID-I/P)*. Biometrics Research, New York State Psychiatric Institute, New York.
- Fitzsimmons, J., Kubicki, M., Smith, K., Bushell, G., Estepar, R.S., Westin, C.F., Nestor, P.G., Niznikiewicz, M.A., Kikinis, R., McCarley, R.W., Shenton, M.E., 2009. Diffusion tractography of the fornix in schizophrenia. *Schizophr. Res.* 107, 39–46.
- Foong, J., Symms, M.R., Barker, G.J., Maier, M., Miller, D.H., Ron, M.A., 2002. Investigating regional white matter in schizophrenia using diffusion tensor imaging. *Neuroreport* 13, 333–336.
- Fraley, C., Raftery, A.E., 1998. How many clusters? Which clustering method? Answers via model-based cluster analysis. *Comput. J.* 41, 578–588.
- Fred, A.L., Jain, A.K., 2005. Combining multiple clusterings using evidence accumulation. *IEEE Trans. Pattern Anal. Mach. Intell.* 27, 835–850.
- Freitas, A.A., 2004. A critical review of multi-objective optimization in data mining: a position paper. *SIGKDD Explor.* 6, 77–82.
- Gallichan, D., Scholz, J., Bartsch, A., Behrens, T.E., Robson, M.D., Miller, K.L., 2010. Addressing a systematic vibration artifact in diffusion-weighted MRI. *Hum. Brain Mapp.* 31, 193–202.
- Haijma, S.V., Van Haren, N., Cahn, W., Koolschijn, P.C., Hulshoff Pol, H.E., Kahn, R.S., 2013. Brain volumes in schizophrenia: a meta-analysis in over 18,000 subjects. *Schizophr. Bull.* 39, 1129–1138.
- Harari, O., Park, S.Y., Huang, H., Groisman, E.A., Zwir, I., 2010. Defining the plasticity of transcription factor binding sites by Deconstructing DNA consensus sequences: the PhoP-binding sites among gamma/enterobacteria. *PLoS Comput. Biol.* 6, e1000862.
- Hartigan, J., Wong, M., 1979. Algorithm AS 136: a K-means clustering algorithm. *Appl. Stat.* 100–108.
- Holliday, E.G., McLean, D.E., Nyholt, D.R., Mowry, B.J., 2009. Susceptibility locus on chromosome 1q23–25 for a schizophrenia subtype resembling deficit schizophrenia identified by latent class analysis. *Arch. Gen. Psychiatry* 66, 1058–1067.
- Huang, H., Fan, X., Williamson, D.E., Rao, U., 2011. White matter changes in healthy adolescents at familial risk for unipolar depression: a diffusion tensor imaging study. *Neuropsychopharmacology* 36, 684–691.
- Jech, T., 2003. *Set Theory: The Third Millennium Edition, Revised and Expanded*. Springer.
- Keller, T.A., Kana, R.K., Just, M.A., 2007. A developmental study of the structural integrity of white matter in autism. *Neuroreport* 18, 23–27.
- Kubicki, M., Shenton, M.E., 2014. Diffusion tensor imaging findings and their implications in schizophrenia. *Curr. Opin. Psychiatry* 27, 179–184.
- Kubicki, M., McCarley, R., Westin, C.F., Park, H.J., Maier, S., Kikinis, R., Jolesz, F.A., Shenton, M.E., 2007. A review of diffusion tensor imaging studies in schizophrenia. *J. Psychiatr. Res.* 41, 15–30.
- Kumar, J., Iwabuchi, S., Oowise, S., Balani, V., Palaniyappan, L., Liddle, P.F., 2015. Shared white-matter dysconnectivity in schizophrenia and bipolar disorder with psychosis. *Psychol. Med.* 45, 759–770.
- Latorre Carmona, P., Sánchez, J.S., Fred, A.L.N., SpringerLink (Online service), 2013. *Mathematical Methodologies in Pattern Recognition and Machine Learning Contributions from the International Conference on Pattern Recognition Applications and Methods, 2012*. Springer Proceedings in Mathematics & Statistics, Springer New York: Imprint: Springer, New York, NY, pp. VIII, 194 p. 158 illus., 140 illus. in color.
- Lee, D.D., Seung, H.S., 1999. Learning the parts of objects by non-negative matrix factorization. *Nature* 401, 788–791.
- Lee, S.H., Kubicki, M., Asami, T., Seidman, L.J., Goldstein, J.M., Mesholam-Gately, R.I., McCarley, R.W., Shenton, M.E., 2013. Extensive white matter abnormalities in patients with first-episode schizophrenia: a diffusion tensor imaging (DTI) study. *Schizophr. Res.* 143, 231–238.
- Lim, K.O., Hedehus, M., Moseley, M., de Crespigny, A., Sullivan, E.V., Pfefferbaum, A., 1999. Compromised white matter tract integrity in schizophrenia inferred from diffusion tensor imaging. *Arch. Gen. Psychiatry* 56, 367–374.



- Liu, X., Lai, Y., Wang, X., Hao, C., Chen, L., Zhou, Z., Yu, X., Hong, N., 2013. Reduced white matter integrity and cognitive deficit in never-medicated chronic schizophrenia: a diffusion tensor study using TBSS. *Behav. Brain Res.* 252, 157–163.
- Madeira, S.C., Oliveira, A.L., 2004. Biclustering algorithms for biological data analysis: a survey. *IEEE/ACM Trans. Comput. Biol. Bioinform.* 1, 24–45.
- Minami, T., Nobuhara, K., Okugawa, G., Takase, K., Yoshida, T., Sawada, S., Ha-Kawa, S., Ikeda, K., Kinoshita, T., 2003. Diffusion tensor magnetic resonance imaging of disruption of regional white matter in schizophrenia. *Neuropsychobiology* 47, 141–145.
- Mitchell, T.M., 1997. *Machine Learning*. McGraw-Hill, New York.
- Mori, S., 2007. *Introduction to Diffusion Tensor Imaging*. Elsevier Science & Technology, Amsterdam, NLD.
- Nacsa, J., Radaelli, A., Edghill-Smith, Y., Venzon, D., Tsai, W.P., Morghen Cde, G., Panicali, D., Tartaglia, J., Franchini, G., 2004. Avipox-based simian immunodeficiency virus (SIV) vaccines elicit a high frequency of SIV-specific CD4+ and CD8+ T-cell responses in vaccinia-experienced SIVmac251-infected macaques. *Vaccine* 22, 597–606.
- Ozelik-Eroglu, E., Ertugrul, A., Oguz, K.K., Has, A.C., Karahan, S., Yazici, M.K., 2014. Effect of clozapine on white matter integrity in patients with schizophrenia: a diffusion tensor imaging study. *Psychiatry Res.* 223, 226–235.
- Pascual-Montano, A., Carazo, J.M., Kochi, K., Lehmann, D., Pascual-Marqui, R.D., 2006a. Nonsmooth nonnegative matrix factorization (nsNMF). *IEEE Trans. Pattern Anal. Mach. Intell.* 28, 403–415.
- Pascual-Montano, A., Carmona-Saez, P., Chagoyen, M., Tirado, F., Carazo, J.M., Pascual-Marqui, R.D., 2006b. bioNMF: a versatile tool for non-negative matrix factorization in biology. *BMC Bioinforma.* 7, 366.
- Poudel, G.R., Stout, J.C., Dominguez, D.J., Churchyard, A., Chua, P., Egan, G.F., Georgiou-Karistianis, N., 2015. Longitudinal change in white matter microstructure in Huntington's disease: the IMAGE-HD study. *Neurobiol. Dis.* 74, 406–412.
- Rissanen, J., 1989. *Stochastic Complexity in Statistical Inquiry*. World Scientific, Singapore.
- Romero-Zalaz, R.C., Rubio, R., Cordón, O., Cobb, P., Herrera, F., Zwir, I., 2008a. A multi-objective evolutionary conceptual clustering methodology for gene annotation within structural databases: a case of study on the gene ontology database. *IEEE Trans. Evol. Comput.* 12 (6), 679–701.
- Romero-Zalaz, R., Del Val, C., Cobb, J.P., Zwir, I., 2008b. Onto-CC: a web server for identifying gene ontology conceptual clusters. *Nucleic Acids Res.* 36, W352–W357.
- Ruspini, E.H., Zwir, I., 2002. Automated generation of qualitative representations of complex objects by hybrid soft-computing methods. In: Pal, S.K., Pal, A. (Eds.), *Pattern Recognition: From Classical to Modern Approaches*. World Scientific, New Jersey, pp. 454–474.
- Shepherd, A.M., Laurens, K.R., Matheson, S.L., Carr, V.J., Green, M.J., 2012. Systematic meta-review and quality assessment of the structural brain alterations in schizophrenia. *Neurosci. Biobehav. Rev.* 36, 1342–1356.
- Sivagnanasundaram, S., Crossett, B., Dedova, I., Cordwell, S., Matsumoto, I., 2007. Abnormal pathways in the genu of the corpus callosum in schizophrenia pathogenesis: a proteome study. *Proteomics Clin. Appl.* 1, 1291–1305.
- Skudlarski, P., Schretlen, D.J., Thaker, G.K., Stevens, M.C., Keshavan, M.S., Sweeney, J.A., Tamminga, C.A., Clementz, B.A., O'Neil, K., Pearlson, G.D., 2013. Diffusion tensor imaging white matter endophenotypes in patients with schizophrenia or psychotic bipolar disorder and their relatives. *Am. J. Psychiatry* 170, 886–898.
- Smith, S.M., 2002. Fast robust automated brain extraction. *Hum. Brain Mapp.* 17, 143–155.
- Smith, S.M., Jenkinson, M., Johansen-Berg, H., Rueckert, D., Nichols, T.E., Mackay, C.E., Watkins, K.E., Ciccarelli, O., Cader, M.Z., Matthews, P.M., Behrens, T.E., 2006. Tract-based spatial statistics: voxelwise analysis of multi-subject diffusion data. *NeuroImage* 31, 1487–1505.
- Sokal, R.R., Michener, C.D., 1958. A statistical method for evaluating systematic relationships. *Univ. Kansas Sci. Bull.* 38, 1409–1438.
- Song, S.K., Sun, S.W., Ramsbottom, M.J., Chang, C., Russell, J., Cross, A.H., 2002. Dysmyelination revealed through MRI as increased radial (but unchanged axial) diffusion of water. *NeuroImage* 17, 1429–1436.
- Spalletta, G., De Rossi, P., Piras, F., Iorio, M., Dacquino, C., Scanu, F., Girardi, P., Caltagirone, C., Kirkpatrick, B., Chiapponi, C., 2015. Brain white matter microstructure in deficit and non-deficit subtypes of schizophrenia. *Psychiatry Res.* 231, 252–261.
- Suddath, R.L., Christison, G.W., Torrey, E.F., Casanova, M.F., Weinberger, D.R., 1990. Anatomical abnormalities in the brains of monozygotic twins discordant for schizophrenia. *N. Engl. J. Med.* 322, 789–794.
- Tamayo, P., Scanfeld, D., Ebert, B.L., Gillette, M.A., Roberts, C.W., Mesirov, J.P., 2007. Metagene projection for cross-platform, cross-species characterization of global transcriptional states. *Proc. Natl. Acad. Sci. U. S. A.* 104, 5959–5964.
- Tavazoie, S., Hughes, J.D., Campbell, M.J., Cho, R.J., Church, G.M., 1999. Systematic determination of genetic network architecture. *Nat. Genet.* 22, 281–285.
- Whitford, T.J., Grieve, S.M., Farrow, T.F., Gomes, L., Brennan, J., Harris, A.W., Gordon, E., Williams, L.M., 2007. Volumetric white matter abnormalities in first-episode schizophrenia: a longitudinal, tensor-based morphometry study. *Am. J. Psychiatry* 164, 1082–1089.
- Wible, C.G., Shenton, M.E., Hokama, H., Kikinis, R., Jolesz, F.A., Metcalf, D., McCarley, R.W., 1995. Prefrontal cortex and schizophrenia. A quantitative magnetic resonance imaging study. *Arch. Gen. Psychiatry* 52, 279–288.
- Zwir, I., Huang, H., Groisman, E.A., 2005a. Analysis of differentially-regulated genes within a regulatory network by GPS genome navigation. *Bioinformatics* 21, 4073–4083.
- Zwir, I., Shin, D., Kato, A., Nishino, K., Latifi, T., Solomon, F., Hare, J.M., Huang, H., Groisman, E.A., 2005b. Dissecting the PhoP regulatory network of *Escherichia coli* and *Salmonella enterica*. *Proc. Natl. Acad. Sci. U. S. A.* 102, 2862–2867.